Volumetric Ultrasound Localization Microscopy

Denis, Louise; Chabouh, Georges; Heiles, Baptiste; Couture, Olivier

DOI
10.1109/TUFFC.2024.3485556

Publication date
2024

Document Version
Final published version

Published in
IEEE Transactions on Ultrasonics, Ferroelectrics, and Frequency Control

Volumetric Ultrasound Localization Microscopy

Louise Denis, *Member, IEEE*, Georges Chabouh, *Member, IEEE*, Baptiste Heiles, *Member, IEEE*, and Olivier Couture, *Member, IEEE*

***Abstract*—Super-resolution ultrasound (SRUS) has evolved significantly with the advent of ultrasound localization microscopy (ULM). This technique enables subwavelength resolution imaging using microbubble contrast agents. Initially confined to 2-D imaging, ULM has progressed toward volumetric approaches, allowing for comprehensive 3-D visualization of microvascular networks. This review explores the technological advancements and challenges associated with volumetric ULM, focusing on key aspects such as transducer design, acquisition speed, data processing algorithms, or integration into clinical practice. We discuss the limitations of traditional 2-D ULM, including dependence on precise imaging plane selection and compromised resolution in microvasculature quantification. In contrast, volumetric ULM offers enhanced spatial resolution and allows motion correction in all directions, promising transformative insights into microvascular pathophysiology. By examining current research and future directions, this review highlights the potential of volumetric ULM to contribute significantly to diagnostic across various medical conditions, including cancers, arteriosclerosis, strokes, diabetes, and neurodegenerative diseases.**

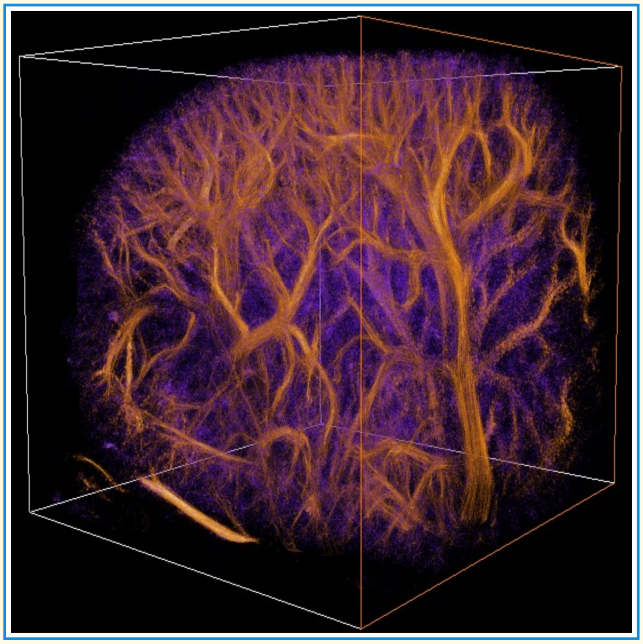

***Index Terms*— Fully addressed, multiplexed, row–column array, sparse array, super-resolution ultrasound (SRUS), volumetric ultrasound localization microscopy (ULM).**

I. Introduction

SUPER-RESOLUTION ultrasound (SRUS) is an imaging modality defined by its capacity to distinguish objects and phenomena closer than the classical diffraction limit [1], [2]. Several techniques can now achieve such subwavelength resolution, sometimes micrometric, including fluctuation-based imaging (SUSHI) [3], [4], structured insonification [5], and ultrasound localization microscopy (ULM) [6].

In particular, ULM relies on the localization of separable microscopic acoustic scatterers and the accumulation of their subwavelength positions or tracks [7], [8]. To date, ULM has most commonly relied on injectable microbubbles known as ultrasound contrast agents, to highlight the microcirculation [9]. Other ongoing studies are focused on the development of more sophisticated contrast agents, with the goal of extending their in vivo presence and enhancing ultrasonic detection sensitivity [11].

ULM has since been demonstrated in vitro, in vivo, and clinically [12], [13]. This technique has shown its ability to map microvasculature in a multitude of organs, such as the brain [14], kidney [15], [16], [17], liver [18], pancreas [18], transfontanellar brain [19], lymph nodes [21], heart [20] (with SRUS software), and testicles [22], as well as in a collection of diseases such as cancer [23], stroke [24], ischemic heart disease [25], and chronic kidney disease [26]. As a token of the importance that super-resolution has taken in the ultrasound community, there is an increasing effort to standardize methods, as well as openly share data and algorithms (PALA [27] and Akebia [16], [28]). This is in part due to the emergence of deep-learning methods that need to be trained on big datasets [29] and call for realistically simulated data with access to ground truth [30], [31].

Performed at various imaging speeds, ranging from more conventional clinical frame rates (a few images per second) to high-frame rates (above 500 frames/s), the vast majority

Received 3 October 2024; accepted 21 October 2024. Date of publication 25 October 2024; date of current version 10 January 2025. This work was supported in part by European Research Council (ERC) through European Union Horizon 586 H2020 Program/ERC Consolidator under Grant 772786-ResolveStroke. *(Louise Denis and Georges Chabouh contributed equally to this work.) (Corresponding author: Georges Chabouh.)*

Louise Denis, Georges Chabouh, and Olivier Couture are with the Laboratoire d'Imagerie Biomédicale, CNRS, INSERM, Sorbonne University, 75006 Paris, France (e-mail: louise.denis@sorbonne-universite.fr; georges.chabouh@sorbonne-universite.fr; olivier.couture@sorbonne.universite.fr).

Baptiste Heiles is with the Division of Chemistry and Chemical Engineering, California Institute of Technology, Pasadena, CA 91125 USA, and also with the Department of Imaging Physics, Delft University of Technology, 2628 CD Delft, The Netherlands (e-mail: baptiste.heiles@gmail.com).

Digital Object Identifier 10.1109/TUFFC.2024.3485556

Highlights

- **We review volumetric ULM, focusing on its technology, capabilities, key metrics, and tradeoffs.**
- **Clinical applications could use volumetric approaches to overcome 2-D ULM limitations such as user dependence, out-of-plane motion artifacts, and inaccurate quantification from 2-D projections.**
- **This review covers the technologies used for volumetric ULM, along with discussions on its applications, limitations, technological advancements, and future developments.**

of ULM studies have been implemented in two dimensions. In conventional clinical systems, the extraction of ultrasound contrast agent signals has been performed with specific nonlinear sequences, such as pulse inversion or amplitude modulation, which provided a high contrast-to-tissue ratio [32]. However, ultrafast sequences have enhanced sensitivity to fast flows, making these flows more detectable by ULM when filtered by frequency or spatiotemporal filters [18], [33], [34]. Nevertheless, fast flows usually happen in large vessels that can also be detected by the Doppler method, and ULM usually shows most of its significance in reconstructing and distinguishing small vessels.

In some of these studies, ULM achieves a resolution of a tenth of the wavelength. For high frequencies (>15 MHz), this is very close to the diameter of the perfused microbubbles. While this resolution is not to be mistaken for the ability to map vessels this size, it certainly brings ultrasound closer to being able to detect capillaries. However, it also creates a new set of tradeoffs as nature is stingy with gratuitous midday meals, between spatial resolution and saturation, i.e., temporal resolution. For instance, the main assumption of ULM is that microbubbles can be individually isolated and localized [7]. Since the formation of a super-resolved image relies on the presence of a microbubble in each pixel, it ties resolution and saturation together with detection. As the pixel size is reduced to achieve super-resolution, the likelihood of a microbubble passage diminishes and accumulation times lengthen [35]. Considering the rarity of microbubbles—a few hundred million microbubbles per injection with respect to tens of trillions of red blood cells—and the flow rate in the smallest capillaries and arterioles, ULM's temporal resolution is ultimately linked to a physiological determinant [see Fig. 1(c)].

Plagued by this new balance between acquisition time and temporal resolution, ULM is more difficult to implement than conventional 2-D ultrasound B-mode and Doppler scanning in a clinical setting. One direction is to continue performing handheld scanning in real time and risk out-of-plane motion [see Fig. 1(b)], thereby limiting resolution gains. Another direction is to generate high-quality images with longer acquisition times and motionless organs if possible. However, 2-D imaging restricts the ability to fully correct for motion, and exploring a full organ through plane-by-plane acquisitions is a tedious and not always feasible process. Moreover, blood flow quantification is inherently flawed as the 3-D path of each microbubble is projected in two dimensions. As one of the strengths of ULM is the capacity to measure positions and quasi-isotropic velocities in blood flow at the micrometer and millimeter/second scale, such elevation projection, i.e., due to the 2-D, reduces the scope of the biomarkers that could be extracted from ULM [see Fig. 1(a)]: out-of-plane vessels will lead to bias in biomarkers estimation. Finally, 2-D approaches require the plane of interest to be selected prior to the ULM imaging, which increases user dependence, which is already a fundamental drawback of ultrasound imaging.

The quest for volumetric ultrasound imaging was initiated decades ago by Von Ramm and Smith [36], but it appears that ULM would particularly benefit from a volumetric approach. In this review, we will refer to techniques where each single microbubble can be localized with enhanced resolution in the three directions of space at any time of the acquisition as volumetric ULM. This definition excludes, for example, plane-by-plane (2-D + translation) reconstruction such as by Errico et al. [6], Lin et al. [37], Zhu et al. [38], Lowerison et al. [39], Ozdemir et al. [40], and Yin et al. [41]. We have also not taken into account the various new technologies enabling ultrasound volumetric acquisitions to be made without ULM, such as in studies presenting the single transducer [42], improvements to the row–column array (RCA) [43], the use of divergent waves [44], or the use of microbeamformer such as in [45].

The main advantage of volumetric ULM is that as the subwavelength position of the microbubble is known, vascular anatomy and blood flow can be reconstructed to a micrometric resolution in all directions. Another advantage is that a larger collection of microbubbles can also be acquired at each timepoint since the field of view is bigger and also because microbubbles are easier to separate due to the added third coordinate. Hence, volumetric ULM can reconstruct a large volume of tissue in less time with improved quantification as shown by Chavignon et al. [46]. Motion correction is also feasible in all three dimensions, and full compensation and reconstruction are possible. Based on our day-to-day experiments, we can also state that volumetric ULM vastly facilitates the positioning of the probe, avoiding the prerequisite of precise imaging plane selection. In the end, volumetric ULM could achieve what is already common in other imaging modalities: an agnostic, blinded acquisition, and offline analysis of an entire organ with careful selection of the imaging region of interest in post-processing.

To achieve volumetric ULM, the imaging system must be capable of focusing at any point in the volume, both in emission and reception, either physically or synthetically. This involves an increase in the total number of transducer elements and electronic lines, naturally leading to higher complexity in manufacturing probes and scanners, acquisition frameworks, and larger beamformed datasets (from gigabytes to terabytes). The potential of volumetric ULM was already perceived at

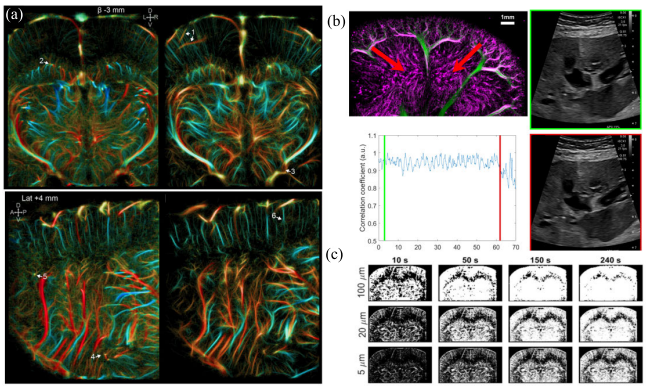

Fig. 1. Limitations of 2-D ULM. (a) Volumetric ULM demonstrating greater microbubble sparsity and more precise vessel hemodynamic rendering: maximum intensity projections of ULM on a 0.2-mm slab (left) versus 2-D ULM from 2-D slices (right) extracted from [46]. 2-D ULM shows out-of-plane vessels that appear brighter due to elevation projection (vessel n°1), poorly tracked (vessel n°2 and n°3), or deleted due to the filter (vessel n°6), copyright IEEE. (b) (Upper left) Out-of-plane artifactual tracks on the rat kidney in the medullary (red arrow) and (bottom left) estimation of movement by cross correlation on the B-mode of a patient kidney: the green line represents the B-mode at 4 s (upper right) and the red line represents the B-mode at 62 s (bottom, right): a slight drift to the right is observed [16], copyright Elsevier. (c) Optimal microbubble concentration for effective ULM acquisition, highlighting the balance between resolution and detection [35], copyright Springer Nature.

the onset of the field by Desailly et al. [47] and O'Reilly and Hynynen [48]. At this point, it was recognized that the echoes of an individual microbubble would have to be intercepted by a receive transducer spread across at least two dimensions, either through parallel multiple linear arrays or a concave multielement array. However, as the localization precision of a single microbubble is affected by the signal-to-noise ratio (SNR) and the point spread function (PSF) of the system, high-quality imaging must be achievable in all directions for volumetric ULM [49].

At the onset of ULM, the necessity for a volumetric version was rapidly identified [47], [48]. However, for in vivo and ultimately clinical transfer, further technological developments were necessary. Building upon volumetric ultrafast scanners and their probes first used by Provost et al. [50], Heiles et al. [51], [52] proposed a system with a fully addressed 8-MHz 32 × 32 matrix connected to a combination of four clinical ultrafast scanners as already used in the same team. After demonstrating in vitro separability of vessels below the wavelength (52 μm), they demonstrated volumetric ULM in the craniotomized rat brain, mapping the vasculature of the entire organ at a resolution between 20 and 30 μm. Since Heiles et al. [51], [52], other systems and applications have been proposed, tackling the various challenges posed by volumetric ULM and opening new venues for diagnostic applications and preclinical studies.

It is our opinion that ULM's clinical application will ultimately rely on volumetric approaches, as it relieves several drawbacks of ULM, as well as the user dependence on ultrasound imaging in general In this review, we extend the description of volumetric ULM, especially its technological implementation, its capabilities, metrics, tradeoffs, and highlight preclinical and clinical studies. We start with an introduction of the technologies used in the field. We discuss the quest for deep-organ (>1 cm) super-resolution vascular imaging, its clinical benefits, and its historical evolution. We then review the applications, the limitations, and the technological perspectives. Finally, we present future endeavors, applications, and necessary evolutions.

II. Technologies

A collection of ultrasound systems and processes has been proposed to perform volumetric ULM, in vitro, in vivo, and in silico. We have identified more than 40 publications describing volumetric ULM. Here, to systematize the review, we chose to classify these articles with respect to the ultrasound emission scheme that they used. The articles discussed in this review are summarized in Table I. Conventionally, an ultrasound probe for volumetric imaging is manufactured by cutting the elements in two orthogonal directions at a scale compatible with ultrasonic beamforming. Bound to the same diffraction laws, the transducer is ideally divided into elements close to half the wavelength for optimized directivity and grating lobe avoidance, sometimes compromising to a wavelength or two wavelengths. Unfortunately, the number of elements of such matrix elements increases quadratically. For example, while a 1-D-array centered around 6 MHz can be 5 cm wide with 256 200-μm elements, a 2-D-array with a 5 × 5 cm footprint at the same center frequency would require 65 000 elements. Without integrated circuits in the probe as in the study by dos Santos et al. [53], the wiring of such a number of elements would be impractical. Various compromises have been proposed, which we will detail in Sections II-A–II-F. It must also be noted that all the techniques presented below are sensitive to the element misalignment of the matrix probe panel, which can be corrected as suggested by McCall et al. [77].

A. Fully Addressed

The first approach presented here is to extend linear arrays in another dimension, mapping a plane with square transducer elements individually connected to a pulse–echo electronic channel. We refer to this technology as fully addressed probes [see Fig. 2(a)]. For instance, a 32 × 32 element matrix probe would comprise 1024 elements, and its imaging field-of-view, even considering a two-wavelength pitch, is fairly restricted to slightly larger than 1 cm across for an 8-MHz array. Because of the directivity of these elements, such a matrix probe is limited to imaging directly below the probe itself.

As each of the N^2 elements requires to be addressed both in emission and in reception at the same time, the number of channels required in the ultrasound scanners increases dramatically. The first systems built with this capability were custom-made research programmable scanners published by Provost et al. [50] and Jensen et al. [54].

This fully addressed system in emission was used by Heiles et al. [51] to produce the volumetric ULM study. A 32 × 32 matrix probe centered at 8 MHz with a 90% bandwidth at −6 dB, a 0.3-mm pitch, and a 0.3-mm element size (Vermon, Tours, France) was driven by such Quadruple-Aixplorer, leading to a volume rate of 500 Hz. In this in

TABLE I
VOLUMETRIC ULM: STATE OF THE ART

Technology	Study	Applications	Probe	Ultrasound System
Fully Addressed	Heiles 2019 [51]	In-vitro agar bifurcation 200 μm	32-by-324 matrix-array (8 MHz)	4 synchronized Aixplorer (Supersonic Imaging)
	Tang 2020 [93]	In-vivo Rat Brain	Spherical array (256 elements) 4 MHz	1 Verasonics 256
	Demeulenaere 2022a [56]	In-vivo Mouse Brain	32-by-354 matrix-array (9 MHz)	4 synchronized Verasonics 256
	Demeulenaere 2022b [25]	Ex-vivo rat heart	32-by-354 matrix-array (9 MHz)	4 synchronized Verasonics 256
	McCall 2023a [57]	In-vivo Rat Brain	32-by-324 matrix-array (7.8 MHz)	4 synchronized Verasonics 256
	McCall 2023b [76]	In-vivo Mouse Brain	32-by-324 matrix-array (7.8 MHz)	4 synchronized Verasonics 256
	Lei 2023 [98]	In-vivo Rabbit Eye	32-by-324 matrix-array (8 MHz)	4 synchronized Verasonics 256
	Heiles 2023 [52]	In-vivo Rat Brain	32-by-354 matrix-array (8 MHz)	4 synchronized Aixplorer (Supersonic Imaging)
	Zhang 2024 [97]	In-vivo rabbit VX2 tumours	32-by-324 matrix-array (7.8 MHz)	4 synchronized Verasonics
Sparse	Harput 2019 [62]	In vitro double helix tubes 200 µm	Sparse array (3.7 MHz)	Synchronized ULA-OP 256 systems
	O'Reilly 2013 [48]	In-vitro through human skullcap	Spherical array (128 elements) 612 kHz	A custom-made system
	Foroozan 2018 [59]	In-vitro through human skullcap	Spherical array (128 elements) 612 kHz	1 Verasonics (Vantage 128)
	Robin 2021 [64]	In-vivo Mouse Brain	Spherical array (512 elements) 5 MHz	A custom-made system
	Wei 2023 [94]	In-vivo Porcine Kidney	Homemade sparse array 5 MHz	1 Verasonics (Vantage 256)
	Deng 2023 [60]	In-vivo Rabbit Brain	Homemade spherical phased array (306, 612, and 1224 kHz)	1 Verasonics (Vantage 256)
Multiplexed	Chavignon 2021 [67]	In-vivo Rat Brain	32-by-35* matrix-array (7.8 MHz)	1 Verasonics 4-to-1 MUX
	Chavignon 2022 [24]	In-vivo Rat Brain	32-by-32* matrix-array (7.8 MHz)	1 Verasonics 4-to-1 MUX
	Lok 2022 [68]	Ex-ovo Chicken Embryo Brain	32-by-35* matrix-array (7.8 MHz)	1 Verasonics 4-to-1 MUX
	Yan 2023 [69]	In-vivo Rat Kidney	32-by-35* matrix-array (7.8 MHz)	1 Verasonics 4-to-1 MUX
	Ghigo 2024 [72]	In-vivo Cat & Mouse Brain	32-by-35* matrix-array (7.8 MHz)	1 Verasonics 4-to-1 MUX
	Bourquin 2024 [71]	In-vivo Cat & Mouse Brain	32-by-35* matrix-array (7.8 MHz)	1 Verasonics 4-to-1 MUX
	Riemer 2023 [70]	In-vivo Rabbit Kidney & Mouse Brain	32-by-35* matrix-array (7.8 MHz)	1 Verasonics 4-to-1 MUX
	Chabouh Denis 2024 [95]	In-vivo Rat Kidney	32-by-35* matrix-array (7.8 MHz)	1 Verasonics 4-to-1 MUX
	Coudert 2024a [74]	In-vitro Latex tube in agar	32-by-35* matrix-array (1.5 MHz)	1 Verasonics 4-to-1 MUX
	Coudert 2024b [75]	In-vivo Sheep Brain	32-by-35* matrix-array (1.5 MHz)	1 Verasonics 4-to-1 MUX
	Xing 2024 [73]	In-vivo Macaque Brain	32-by-35* matrix-array (7.8 & 1.5 MHz)	1 Verasonics 4-to-1 MUX
	Chabouh 2024 [113]	In-vivo Rat Kidney	32-by-35* matrix-array (7.8 & 1.5 MHz)	1 Verasonics 4-to-1 MUX
	Chabouh 2024 [114]	Awake mouse brain	32-by-35* matrix-array (7.8 & 1.5 MHz)	1 Verasonics 4-to-1 MUX
Row-Column	Jensen 2019 [78]	In-vitro micro-phantom	62+62 RC (3 MHz)	SARUS experimental scanner
	Ommen 2021 [82]	In-vitro 3D printed structures	62+62 RC (3 MHz)	SARUS experimental scanner
	Jensen 2022 [83]	In-vivo Rat Kidney	128+128 (6 MHz)	1 Verasonics (Vantage 256)
	Hansen-Shearer 2024 [84]	Rabbit Kidney & Human thyroid	128+128 (3 MHz)	1 Verasonics (Vantage 256)
	Caudoux 2024 [85]	Ex-vivo heart	96+64 Curved toroidal RC	1 Verasonics (Vantage 256)
	Wu 2024 [10]	In-vivo Mouse Brain	128+128 (12 MHz)	1 Verasonics (Vantage 256)
Large Elements	Favre 2022 [88]	Simulations	10cm x 10 cm 256 elements (1 MHz)	Field II
	Favre 2023 [89]	In-vitro	4x4 matrix-array (16 elements) 950 kHz	1 Verasonics (Vantage 256)
Simulations	Belgharbi 2023 [31]	Based on 2-photon microscopy	32-by-35* matrix-array (8 & 3 MHz)	SIMUS
	McCall 2021 [90]	Phase abberation	N/A	Fullwave
	Rauby 2024 [91]	Neural Network to reduce memory	32-by-35* matrix-array (7.8 MHz)	Belgharbi 2023 [31]

*Note: 1024 matrix probes can either be referred as 32 $\times$ 32 or 32 $\times$ 35 due to the 3 free lines of elements between panels.

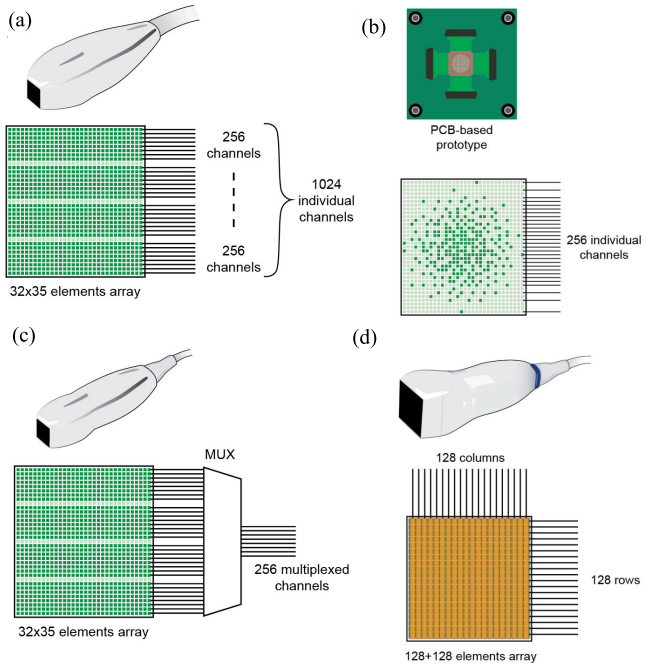

Fig. 2. Common ultrasound systems for volumetric ULM. (a) Fully addressed system. (b) Sparse array system. (c) Matrix probe with a multiplexed system. (d) Row–column array. Note that 1024 matrix probes can either be referred to as 32 × 32 or 32 × 35 due to the three free lines of elements between panels.

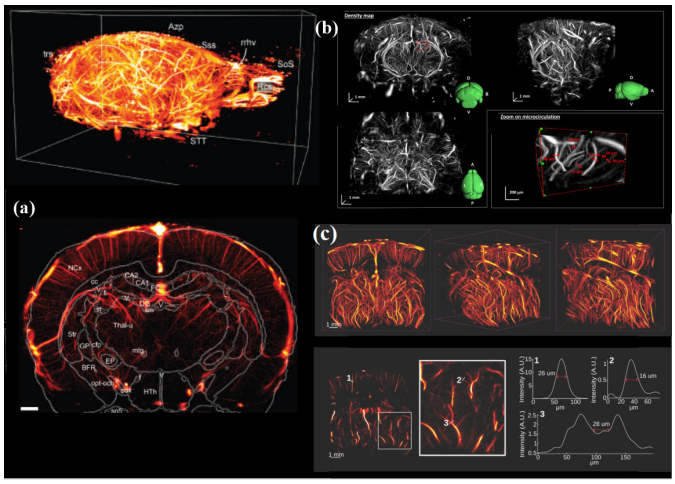

Fig. 3. Fully addressed system for volumetric ULM. (a) Mapping the entire rat brain vasculature at a resolution between 20 and 30 μm [52], [55] with permission. (b) Transcranial ULM in mouse brain [56], copyright Elsevier. (c) Transcranial ULM in rat brain [57], copyright Theranostics.

vitro study, a 3-D y-shaped canal has been reconstructed with separation between each branch down to 52 μm, more than a sixfold improvement in resolution. The same fully addressed system was then used for the first in vivo volumetric ULM in the rat brain with full skull removal [2], [52], [55] [see Fig. 3(a)].

Later, four identical programmable ultrasound scanners (Vantage 256, Verasonics, Kirkland, WA, USA) were synchronized to achieve 1024 fully addressed elements in transmission and in reception, with a volume rate of 750 Hz, to achieve volumetric ULM: transcranial for brain microvasculature in mice by Demeulenaere et al. [56] and in rats by McCall et al. [57] [see Fig. 3(b) and (c), respectively].

The main advantage of fully addressed systems is that the entire imaging zone can be illuminated in a single transmit/receive operation. The volume rate achieved by this type of system is, therefore, comparable to 2-D ultrafast ultrasound, making it possible to capture very rapid phenomena, such as those observed in the blood flow of major arteries or within the heart. The disadvantages of this approach are the prohibitive cost of building custom machines with such a high number of channels and their limited applicability in a clinical setting where machines need to be certified to ensure the safety of the medical staff and patients. Their size also makes them less portable.

B. Sparse

One possible solution for limiting the number of channels, and therefore reducing the electronic complexity behind them, is sparse addressing. The piezo-electric elements used are still contained in a matrix and of isotropic dimensions, but only a subset is electronically addressed. The technology relies on destroying the periodicity of an underpopulated array while carefully selecting the distribution of addressed elements to maintain the same aperture width, as explained by Turnbull and Foster [58] [see Fig. 2(b)].

A first demonstration of volumetric ULM with a sparse array imaged a spiral tube phantom through an ex vivo human skullcap with three folds higher resolution, i.e., O'Reilly and Hynynen [48] [see Fig. 4(a)]; 128 elements were randomly selected from a 1372-element (pseudorandom) hemispherical transcranial therapy array at a center frequency of 612 kHz. Inspired by optical super-resolution techniques such as photo-activated localization microscopy (PALM), a passive acoustic mapping (PAM) combined with 3-D Gaussian fitting was used to sublocalize the microbubble PSF to monitor therapy.

Following O'Reilly and Hynynen [48]. Foroozan et al. [59] employed the same setup with an optimized sparse arrangement to compare the localization approach with a deconvolution-based method. Inspired by stochastic optical resolution microscopy (STORM), they estimate the maximum likelihood map from each volume in the acquisition sequence based on deconvolution with a PSF model. This alternative method has the advantage of not requiring localization. In another study [60], a multifrequency piezo-electric element was used to develop transcranial ULM in the rabbit using vaporized nanodroplets.

Robin et al. [64] showed volumetric ULM in vitro (agar-based tissue mimicking phantom) and in vivo transcranial in mice, combined with photoacoustic tomography [see Fig. 4(b)]. Volumetric ULM with a sparse array driven by the ULA-OP 256 research scanner [61] was employed by Harput et al. [62] in vitro in 200-μm tubes arranged in a double helix shape [see Fig. 4(c)]. In [63], 512 elements were selected in a density-tapered 2-D spiral layout from a 32 × 32 matrix array driven at 3.7 MHz. A spherical array of

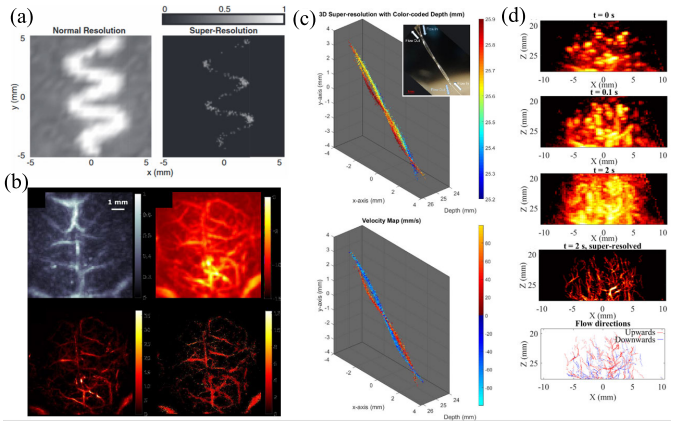

Fig. 4. Sparse array system for volumetric ULM. (a) Demonstration of volumetric ULM using a sparse array to image a spiral tube phantom through an ex vivo human skullcap [48], copyright Medical Physics. (b) Combined photoacoustic and super-resolution imaging to measure oxygen saturation several centimeters deep in rodent brains using spherical sparse array [64], copyright IEEE. (c) In vitro ULM with a sparse array imaging 200-μm tubes arranged in a double helix [62], copyright IEEE. (d) In vivo volumetric ULM in porcine kidney using a homemade sparse array in a tapering spiral pattern centered at 5 MHz [94], copyright Elsevier.

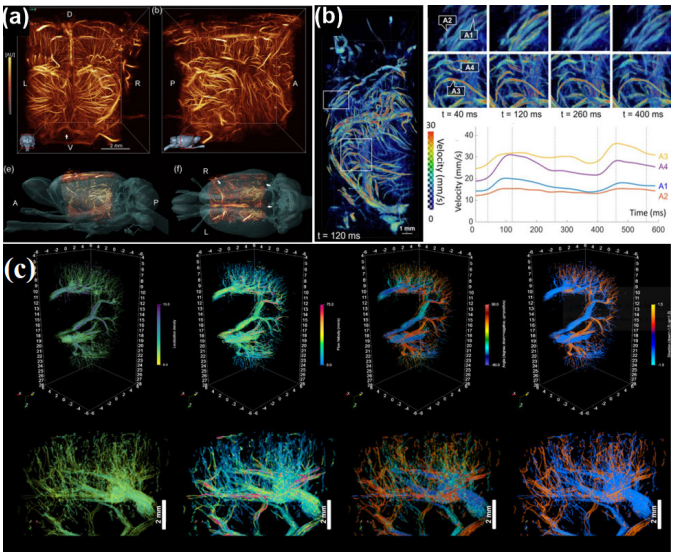

Fig. 5. Multiplex system for volumetric ULM. (a) Demonstration of volumetric ULM using a multiplexed system, showing in vitro and in vivo transcranial imaging in rat brains [67], copyright IEEE. (b) dULM to measure in vivo pulsatility in mouse and cat brains, with simultaneous ECG monitoring [71], copyright IOP Publishing. (c) Volumetric ULM with phase change contrast agents in rabbit kidney [70], copyright Wolters Kluwer Health, Inc., Waltham, MA, USA.

512 elements driven at 5 MHz was used, with only the central 256 elements used for ultrasound imaging. Finally, Wei et al. [94] used a homemade sparse array in a tapering spiral pattern and centered at 5 MHz for in vivo volumetric ULM in porcine kidney [see Fig. 4(d)].

Using sparse array technology, the acquisition speed remains similar to that of direct addressing, while data quantity and system complexity are reduced, i.e., a single 256-channel echograph is required to address 256 transducers. Sparse arrays have been shown to yield good lateral resolution in 3-D, i.e., reduction in the width of the main lobe, when the active element mapping is optimized. However, the contrast-to-noise ratio is inevitably reduced compared to a fully addressed approach due to the reduced active aperture. This approach has a tremendous advantage compared to fully addressed when it comes to diverging waves as proven by Roux et al. [101]. The downside of sparse arrays is that the architecture offers much less flexibility than fully addressed arrays since the mapping needs to be decided beforehand, thus limiting insonification patterns.

C. Multiplexed

Another solution to reduce the number of channels while maintaining isotropic resolution and mapping the entire probe fingerprint is to use each electronic channel to address multiple elements. The selection of the element during transmit or receive is done through a series of channel switches called a multiplexer [see Fig. 2(c)]. A fairly common multiplexed approach utilizes transmit/receive patterns of four groups of 256 elements to address a previously mentioned fully populated 1024-element array, as shown by Bernal et al. [65]. Any type of probe can use a multiplexer, not only fully populated but also sparse arrays as in [66], which would allow mapping a larger field of view than a fully populated array while maintaining a low channel count.

The first volumetric ULM demonstration with a multiplexed system was proposed by Chavignon et al. [67] and was tested in vitro using an agar-based tissue-mimicking phantom (wallless tube size of 0.5 mm) and in vivo in the transcranial rat brain [see Fig. 5(a)]. A 32 $\times$ 32 matrix probe of 1024 elements is driven at a central frequency of 7.8 MHz with a single Vantage 256[1] Research Ultrasound System (Verasonics, Inc., Kirkland, WA, USA) via the Verasonics UTA 1024-MUX adapter. Similar system and probe were employed for volumetric ULM in various studies: in vitro (380 μm flow channel phantom) and ex vivo (chicken embryo brain) by Lok et al. [68], in vivo in the rabbit kidney with various adaptive beamforming techniques by Yan et al. [69], or with sparsely activated phase-change contrast agents by Riemer et al. [70] [see Fig. 5(c)].

Dynamic volumetric ULM (volumetric dULM) was conducted using the same multiplexed system to measure in vivo pulsatility in the mouse (intact skull) and cat (with craniectomy) brain, with and without ECG-triggered ultrasound acquisition, as shown by Bourquin et al. [71] and Ghigo et al. [72] [see Fig. 5(b)]. Volumetric ULM in the macaque brain with and without craniectomy was done by Xing et al. [73] with the multiplexed system at a high frequency of 7.8 MHz and at a lower one, i.e., 3 MHz. Coudert et al. [74] introduced diverging cylindrical waves in the multiplexed system to increase SNR and volume rate in vitro. The same sequence was used to perform volumetric ULM in vivo in sheep brains with a 32 $\times$ 32 matrix probe with central frequency at 1.5 MHz [75]. Finally, McCall et al. [76] used this multiplexed technology to characterize the development of glioblastomas longitudinally in intact-skull mice, while Chabouh et al. [114] developed a

[1]Trademarked.

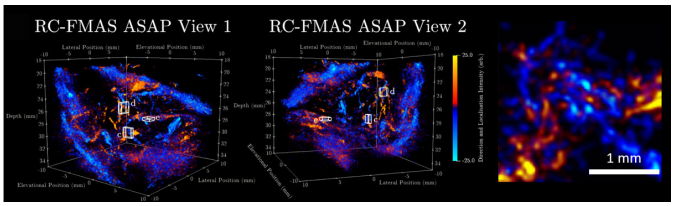

Fig. 6. RCA system for volumetric ULM. Super-resolution projection images of the human thyroid using a large matrix array [84], copyright Elsevier.

stress-free protocol for volumetric transcranial ULM in awake mice.

Employing the multiplexed technique allows for reconstructing the entire volume similar to direct addressing, but the volume rate is at least divided by the multiplexing ratio, limiting the temporal resolution of such approaches. Different pulsing sequences have been studied to reduce the number of emissions needed to insonify and reconstruct the entire volume, from 16 emissions (one per panel with reception by all panels) to four emissions (with reception only by the same panel) [67]. This maintains a high volume rate (>150 volumes/s) with a slight tradeoff in image quality. Interestingly, it was shown that this volumetric ULM technique is sensitive to the mechanical misalignment of the matrix probe panels, which can be corrected, as suggested by McCall et al. [77].

D. Row–Column Addressing

A radical change in the shape of piezoelectric elements can also be a method for reducing channel count and increasing the field of view over fully populated arrays. While most piezoelectric elements are square-shaped, RCA probes use long, thin rectangular elements [see Fig. 2(d)]. Organized in two orthogonal directions, they form a grid with only $N + N$ elements compared to $N \times N$ in a matrix array [78], [79], [80]. Manufacturing rectangular elements is easier than square piezoelectric elements, allowing RCAs to reach a pitch size on the order of the wavelength or half the wavelength to maximize directivity. There are many pulsing sequences that can be used to reconstruct a volume, but the most common ones used for ULM rely on orthogonal plane waves and synthetic apertures, as shown by Flesch et al. [80] and Rasmussen et al. [81].

The first volumetric ULM with an RCA probe was implemented by Jensen et al. [78] at a 3-MHz frequency using a pulse-inversion sequence and demonstrated on 3-D-printed flow microphantoms. Ommen et al. [82] showed that calibrating the RCA pulse sequence with a point phantom led to significant improvement in localization precision. In 2022, the first in vivo demonstration was presented in a rat kidney by Jensen et al. [83]. Hansen-Shearer et al. [84] employed RCA technology with a 3-MHz driving frequency for volumetric ULM in vitro, in vivo rabbit kidney, as well as human thyroid (see Fig. 6). Finally, a curved toroidal RCA probe was used by Caudoux et al. [85] for volumetric ULM in vitro and in a perfused ex vivo heart.

The RCA method enlarges the probe aperture and makes it easier to manufacture probes with a reduced number and complexity of components. Nevertheless, this technique requires a large number of emissions to achieve a sufficient SNR compared to a multiplexed array, thus decreasing the imaging rate. Another disadvantage is the orthotropic nature of the PSF, which contains significant side lobes, impairing the beamformed image quality. Ongoing work is being carried out to repair the PSF [86] diverging lenses, by mechanically curving RCA for a wider field of view as in [85] and [87], or by applying a temporal similarity weighting method to enhance the performance of RCA-based 3-D vascular imaging as in [43].

E. Other Systems

Other systems, including large-element probes as in [88], [89], enable the acquisition of volumes at high imaging rates while maintaining a large field of view. Although these systems exhibit larger side lobes, postprocessing techniques have facilitated in vitro ULM using this matrix type. Clinical systems in which the beamformer is integrated with the ultrasound scanner have also been used to produce volumes at low imaging rates. Although the beamforming steps are not detailed by the manufacturers, this type of acquisition could be used to obtain volumetric ULM.

F. Simulation and Deep Learning

Recent papers on volumetric ULM are based on simulated volumetric data. The creation of this artificial data, using software shown by Belgharbi et al. [31] with SIMUS, enables the study of various postprocessing techniques useful for improving the quality of the final ULM volume. For example, image reconstruction with various adaptive types of beamforming has been tested by Yan et al. [69] and Chabouh et al. [113]. In another publication, the impact of the data acquisition on the degradation of the final image was studied by McCall et al. [90].

These various studies prompt consideration of the emergence of artificial intelligence (AI) in the realm of volumetric ULM. While primarily developed in 2-D, the complexity of the networks and the volume of input data have been significant hurdles, as shown by Rauby et al. [91]. These tools have the potential to overcome several limitations of ULM. Current ULM postprocessing relies on acquisitions lasting several minutes, conducted under conditions of minimal motion and low concentration, to accumulate sufficient data for individual microbubble tracking and vessel reconstruction. However, clinical practice often involves handheld probes, movements perpendicular to the imaging plane, and higher microbubble concentrations due to bolus injections. Shin et al. [29] also showed that AI trained on volumetric data that more closely resemble real-world conditions including movement and high microbubble concentrations holds promise for bridging this gap to medical reality.

III. Applications

The previous section discussed various technologies for volumetric ultrasound, each more or less suited to specific organs or applications. The potential of this technology shall be evaluated based on its capacity to characterize healthy

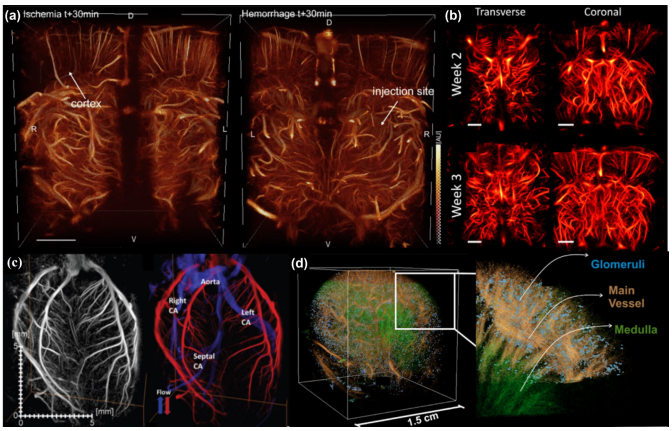

Fig. 7. Applications of volumetric ULM. (a) Transcranial volumetric ULM in rats enabled differentiation between ischemic and hemorrhagic strokes [24], copyright IEEE. (b) Longitudinal study of glioblastoma development in intact-skull mice using volumetric ULM McCall [76], copyright IEEE. (c) Assessment of coronary occlusion dynamics in an ex vivo heart with volumetric ULM Demelanere [10], with permission. (d) Volumetric visualization of glomeruli in rat's kidney with potential implications for diagnosing various pathologies Chabouh [95], copyright IEEE.

organs but primarily on its ability for diagnosis, prognosis, and disease monitoring. Currently, many applications focus on the brain, but abdominal and thoracic uses have also been described.

A. Brain

The brain serves as an ideal preclinical model due to its highly organized vascular structure and the ability to minimize motion thanks to skull immobilization. In the initial study demonstrating volumetric ULM on a large organ, Heiles et al. [27] showed that by acquiring overlapping ULM volumes and registering them in postprocessing, it was possible to map the entire rat brain with minimal motion artifacts. They also highlighted the challenge of brain pulsatility in skull-less models, which can be effectively corrected using high frame rates and 3-D signal acquisition.

In recent a study from McCall et al. [76], based on the previous methodology detailed in [57], the microvasculature of the brain was monitored during the evolution of glioblastoma in a mouse model with an intact skull. A significant reduction in vascular flow was observed within three weeks. The noninvasive and nonionizing nature of volumetric ULM allowed for repeated acquisitions, enabling longitudinal studies. Besides enhancing understanding of neoangiogenesis in tumors, volumetric ULM plays a crucial role in characterizing and monitoring tumor evolution [see Fig. 7(b)].

Another significant application for volumetric ULM could be in stroke diagnosis. For instance, accurately distinguishing between the two most common types of stroke, i.e., ischemic and hemorrhagic, could greatly benefit treatment customization and enhance clinical outcomes for patients. Chavignon et al. [24] advanced this objective by employing transcranial volumetric ULM in rats [see Fig. 7(a)]. In this study, ischemic stroke was induced using the thromboembolic model [92], involving occlusion of the middle cerebral artery through murine thrombin injection. On the other hand, hemorrhagic stroke was induced in the striatum through collagenase injection.

Although these studies were conducted transcranially, it is important to note that rat or mouse skulls are considerably thinner than human skulls. Consequently, several teams have focused on the practical application of transcranial volumetric ULM through thicker skulls and larger brains. O'Reilly and Hynynen [48], followed by Foroozan et al. [59], demonstrated the viability of super-resolution imaging on an in vitro vessel phantom using an ex vivo skull. More recently, Coudert et al. [74] showed the feasibility of volumetric ULM through a considerably thicker sheep skull, up to 7 cm deep. Finally, Xing et al. [73] demonstrated the ability to observe vessels with unprecedented resolution in young macaques to a depth of 3 cm. These diverse studies pave the way for the application of transcranial volumetric ULM in humans, including for stroke and glioblastoma applications.

dULM applied to rat and cat brains by Bourquin et al. [71] and Ghigo et al. [72] has enabled the recovery of ultrasound's dynamic aspect, which is typically lost in traditional ULM due to the need to accumulate data in a fixed area. This technique allows for quantitative measurement of pulsatility, facilitating the differentiation between arteries and veins reconstructed by ULM. It could serve as a diagnostic aid for future medical practitioners, potentially reducing reliance on user interpretation. In addition, dULM holds promise for measuring vessel resistivity, which could aid in the diagnosis of conditions such as stenosis or vasospasm.

Combining ULM with photoacoustics expands the scope of applications for volumetric ULM as shown by Tang et al. [93]. Oxygen saturation measurements in the brain offer additional insights into microvascular visualization. Robin et al. [64] demonstrated the capability to measure oxygen saturation several centimeters deep in rodent brains. Although imaging depth is constrained by light diffraction, this fusion of volumetric ULM with photoacoustics enhances our understanding of vascular physiology.

B. Kidney

To date, volumetric ULM acquisitions have focused exclusively on healthy organs across various animal models, including pig kidneys [94], rabbit kidneys [68], [69], [84], and rodent kidneys [83], [95]. Wei et al. [94] utilized 120/256 transmit/receive elements and 5000-Hz volume rate for Doppler and ULM imaging of the entire left kidney using diverging waves with a 30° opening angle. Recent advancements in volumetric visualization of glomeruli by Chabouh et al. [95] hold promise for diagnosing various pathologies [see Fig. 7(d)]. Longitudinal monitoring of renal failure, diabetes, transplant rejection, and tumors could benefit from counting and tracking these functional renal units.

C. Heart

While the heart presents challenges to most imaging modalities due to significant motion and tissue deformation, 4-D ultrasound imaging has proven particularly beneficial, as

shown by Papadacci et al. [96]. Volumetric ULM demonstrated its capability in assessing coronary occlusion in an ex vivo heart [25]. The study by Demeulenaere et al. [25] achieved occlusion of the left anterior descending artery by ligating it at the basal-mid level of the left ventricle. Furthermore, volumetric ULM enabled investigation of coronary flow dynamics during vasodilation and occlusion in rat hearts [see Fig. 7(c)].

D. Other Microvascular Applications

Zhang et al. [97] utilized volumetric ULM to monitor therapy for subcutaneous carcinoma in rabbits induced by VX2 tissue injection. Five days after administering cisplatin as a therapeutic agent, significant changes in microvessel density and curvature were observed before and after treatment. These volumetric ULM measurements offer longitudinal quantitative information, highlighting the repeatability and efficacy of ULM in assessing therapeutic outcomes.

Despite being complex to set up, volumetric ULM has been successfully applied to the rabbit's eye, facilitated by the low mechanical index permissible through this acoustic window. Lei et al. [98] conducted experiments on healthy tissue, highlighting the potential for volumetric ULM to diagnose various pathologies affecting retinal microcirculation, such as diabetes or hypoxia.

In the future, volumetric ULM is envisioned to play a crucial role in monitoring therapeutic approaches such as in [99] for blood–brain barrier opening. It is also expected to offer a more precise description of functional (fULM introduced by Renaudin et al. [100]) and physiological (sULM, first shown by Denis et al. [16]) processes beyond the diffraction limit.

IV. Challenges and Perspectives

While the field of volumetric ULM is young and still trails its 2-D counterpart in publications and applications, several new directions are emerging due to the third dimension. The expansion of volumetric ULM's scope hinges on several factors: technological democratization, advancements in matrix probes, biomarker definition, modification of diagnostic procedures, and implementation in new applications detailed in subsequent paragraphs.

Volumetric ULM often involves large datasets, sometimes approaching 1 TB/acquisition [52], [57], necessitating research-grade scanners and customized computers. Some clinical scanners can achieve high-volume rates through techniques such as microbeamforming—where part of the beamforming process is integrated electronically into the ultrasound probe. Even if these techniques highly reduce the complexity of the system through prebeamforming neighboring channels (subaperture) in the analog system (before ADC) such as by Larson [112], Guo et al. [45], or dos Santos et al. [53], the recording of tens of thousands of volumes within minutes remains impractical today. Progress in data processing largely follows Moore's law rather than acoustic principles, suggesting that these limitations may be overcome in the coming decades. Addressing data transfer rates will depend on the emergence of new data acquisition cards and innovations from scanner manufacturers.

Beyond electronics, the availability, cost, and quality of matrix probes currently limit volumetric ULM, particularly in research environments. While the cost of conventional linear arrays has decreased due to mass production, 2-D array probes are still custom-made due to their highly specialized architecture and assembly requirements. Compared to 1-D arrays, 2-D arrays generally exhibit lower SNR and probe quality, crucial factors in ULM [49]. Challenges such as element size, matching, ground wiring, and limited electronic channel density continue to hinder volumetric imaging. Advances in transducer technology, including single crystals [102], [111], have shown potential in improving image quality. Further miniaturization of elements and electronics—such as amplification and prebeamforming, will greatly benefit volumetric ULM. The widespread adoption of technologies such as piezoelectric micromachined ultrasound transducers (PMUTs) [103] or capacitive micromachined ultrasonic transducers (CMUTs) [104] and their application to volumetric ULM could rapidly enhance its clinical utility.

Acquisition time remains a significant issue for ULM, whether in 2-D or volumetric formats. The technique often sacrifices temporal resolution for spatial resolution [35]. While faster acquisition methods have been proposed [105], traditional handheld scanning continues to present challenges, balancing acquisition speed with the ability to resolve fine vascular details. Volumetric ULM partially addresses this challenge by allowing more microbubbles to be detected volumetrically compared to a surface. Nevertheless, further research into acquisition procedures will likely be essential for advancing volumetric ULM in the future.

The ULM volumetric visualization is also more challenging than the 2-D one. Whether it is positioning the probe to visualize the target organ or pathology or when visualizing and interpreting the final image, this new volumetric paradigm will require adaptation time and new software to present the data in an optimized and clear way. In terms of probe positioning and target location, several techniques have already been considered, including increasing the divergence of acquisition to avoid missing the target zone [74], [75] or real-time B-mode positioning sequences to reconstruct the orthogonal central planes of the probe, which provides a wealth of information on the entire volume in a relatively short time.

Although several groups have attempted to define biomarkers and quantitative metrics for pathologies visible by volumetric ULM, there is currently no standardized method of quantification used worldwide that goes beyond density or velocity quantification. Besides, some of the biomarkers that have been developed in 2-D must still be translated and proved their worth in volumetric ULM such as the sum of angles metrics used to detect Alzheimer's disease in [39]. Nevertheless, given the expansion of this technique, it is not difficult to imagine a future where common metrics will emerge to quantify microvascular pathologies, as was the case for the resolution definition proposed by Hingot et al. [34].

The clinical translation of volumetric ULM faces many challenges. Key limitations include imaging depth, as organs are larger and deeper, requiring wider probe fields of view, which compromises the quality of the microbubble's PSF and affects localization. In transcranial imaging, bone thickness and structure create significant aberrations, further disrupting microbubble localization. Probe movement, whether due to manual handling or patient factors such as breathing or pathology (e.g., spasms), also complicates acquisition. In addition, ethical hurdles arise since volumetric ultrasound and matrix probes are not routine in clinical practice. Regulations around microbubble injections add to the complexity, limiting the application of volumetric ULM in clinical settings. All in all, beyond motion, attenuation, narrow field of view, and lack of clear disease biomarkers, clinical translation of volumetric ULM is further limited by the unavailability of clinically approved 3-D-capable ultrafast ultrasound scanners that can record long datasets.

The adoption of volumetric ULM has revolutionized the acquisition process in experimental settings. First, positioning is greatly simplified as minor positioning or angular errors have less impact compared to 2-D ULM. The ability to capture a wide volume with a technique that is relatively isotropic in 3-D enables straightforward postprocessing registration, albeit computationally intensive. Furthermore, motion-correction algorithms can be applied in three dimensions to track and correct the movement of microbubbles, overcoming a significant limitation in the subwavelength localization of blood vessels.

Plane selection significantly influences the user's dependence on ultrasound imaging. Volumetric ULM addresses this by enabling the acquisition of a large portion of an organ in a single, albeit lengthy, scan. This approach mirrors MRI or CT scanning, where the subject remains stationary under the matrix probe, while a standardized sequence is initiated alongside contrast agent injection. Parameters are adjusted and images are analyzed post-acquisition across multiple planes, similar to full-body modalities. This retrospective approach to volumetric ULM separates acquisition from analysis, potentially reducing the need for expert radiologists to physically define imaging planes. In addition, ULM's efficient data compression allows for the transmission of processed data to a reference center for further analysis. Thus, volumetric ULM combines the benefits of point-of-care ultrasound with exceptional vascular resolution.

However, realizing the full potential of volumetric ultrasound, especially volumetric ULM, necessitates significant improvements in the imaging field of view and the automation of acquisition settings. Issues such as tissue attenuation or coupling issues can drastically impact image quality, underscoring the need for a thorough assessment of B-mode imaging quality before acquisition. AI, as suggested by Tenajas et al. [106], could aid in assessing image quality and identifying volumes of interest. Expanding the field of view should be pursued through advancements in diverging transducer elements achieved via miniaturization and with RCA. Further technological development on ergodic probes could also simplify the acquisition system [42], [115], [116].

Beyond technical considerations, volumetric ULM must move beyond producing visually appealing images and become a practical diagnostic or preclinical research tool. A critical question arises: what unique insights can volumetric ULM offer that current methods such as CEUS or Doppler cannot? For example, while ULM can depict vessel density, it often parallels conventional scanners in displaying perfusion. Capillaries remain undetected by volumetric ULM, leaving a crucial vascular space unexplored.

The clinical benefits of volumetric ULM are likely to reside deep within the typical voxel size, particularly in phenomena existing at the micrometric scale, which are smoothed over at submillimetric scales by current medical modalities. For example, recent studies using sULM [16] and volumetric sULM [95] have mapped glomeruli, revealing micrometric capillary structures that are normally invisible yet crucial for understanding physiological functions. Oxygen diffusion occurs within tens of microns [107], suggesting that conventional perfusion imaging may not accurately predict oxygenation levels in all cells at all times. Microvascular shunting could increase tissue perfusion heterogeneity [108] while maintaining an appearance of adequate macrometric perfusion. Volumetric ULM has the potential to detect such microperfusion modifications, while classical CEUS cannot.

Due to its exceptional resolution and sensitivity to blood vessels, volumetric ULM could expand the applications of angiography beyond specialized hospital settings. One promising application that we advocate for is the rapid diagnosis of stroke, potentially enabling early treatment [24]. However, as discussed, numerous other applications are conceivable, such as monitoring tumor growth and therapy. The ability to visualize the entire 3-D microvascular environment not only allows for the assessment of angiogenesis progression or regression but also facilitates precise longitudinal follow-up, which is challenging with planar imaging due to the need for micrometric spatial registration [76].

Limits in applying SRUS imaging solely to vessels would be unfortunate, considering that they occupy only a minority of tissue. The use of vaporizable droplets [11] could provide access to extravascular, lymphatic [21], or glymphatic spaces [109]. Super-resolution's definition hinges on resolving subwavelength structures, requiring distinguishable sources that follow reconstructible structures. Achieving localization precision nearing micrometers in certain cases [49] suggests the potential for a cellular version of ULM.

While our review has primarily focused on ULM, exploring a broader range of volumetric SRUS imaging approaches is essential, akin to predecessors in fluctuation imaging (SUSHI) or structured illumination [5]. Similar to optical super-resolution imaging, a diverse array of techniques is necessary to balance tradeoffs among different approaches. For example, the use of contrast agents can significantly affect the applicability of ULM. Shorter acquisitions with limited resolution could also prove beneficial, especially in scenarios where handheld ultrasound imaging is preferred [18].

Finally, the extension of SRUS into the third dimension explores spatial possibilities to their current limits [110]. Now, further exploration should delve into aspects such as

spatial scope, time resolution, and functional and physiological imaging. With a clinical modality capable of discerning tridimensional phenomena at the cellular scale and depths of several centimeters, it is time to steer this ultrasonic volumetric microscope toward new horizons.

REFERENCES

[1] O. Couture, V. Hingot, B. Heiles, P. Muleki-Seya, and M. Tanter, "Ultrasound localization microscopy and super-resolution: A state of the art," *IEEE Trans. Ultrason., Ferroelectr., Freq. Control*, vol. 65, no. 8, pp. 1304–1320, Aug. 2018.

[2] K. Christensen-Jeffries et al., "Super-resolution ultrasound imaging," *Ultrasound Med. Biol.*, vol. 46, no. 4, pp. 865–891, Feb. 2020.

[3] A. Bar-Zion, O. Solomon, C. Tremblay-Darveau, D. Adam, and Y. C. Eldar, "SUSHI: Sparsity-based ultrasound super-resolution hemodynamic imaging," *IEEE Trans. Ultrason., Ferroelectr., Freq. Control*, vol. 65, no. 12, pp. 2365–2380, Dec. 2018.

[4] J. Zhang et al., "Ultrasound microvascular imaging based on super-resolution radial fluctuations," *J. Ultrasound Med.*, vol. 39, no. 8, pp. 1507–1516, Aug. 2020.

[5] T. Ilovitsh, A. Ilovitsh, J. Foiret, B. Z. Fite, and K. W. Ferrara, "Acoustical structured illumination for super-resolution ultrasound imaging," *Commun. Biol.*, vol. 1, no. 1, p. 3, Jan. 2018.

[6] C. Errico et al., "Ultrafast ultrasound localization microscopy for deep super-resolution vascular imaging," *Nature*, vol. 527, no. 7579, pp. 499–502, Nov. 2015.

[7] O. Couture, B. Besson, G. Montaldo, M. Fink, and M. Tanter, "Microbubble ultrasound super-localization imaging (MUSLI)," in *Proc. IEEE Int. Ultrason. Symp.*, Oct. 2011, pp. 1285–1287.

[8] M. Siepmann, G. Schmitz, J. Bzyl, M. Palmowski, and F. Kiessling, "Imaging tumor vascularity by tracing single microbubbles," in *Proc. EEE Int. Ultrason. Symp.*, Oct. 2011, pp. 1906–1909.

[9] G. Chabouh, B. Dollet, C. Quilliet, and G. Coupier, "Spherical oscillations of encapsulated microbubbles: Effect of shell compressibility and anisotropy," *J. Acoust. Soc. Amer.*, vol. 149, no. 2, pp. 1240–1257, Feb. 2021.

[10] A. Wu et al., "3D transcranial dynamic ultrasound localization microscopy in the mouse brain using a row-column array," 2024, *arXiv:2406.01746*.

[11] K. Riemer et al., "Fast and selective super-resolution ultrasound in vivo with acoustically activated nanodroplets," *IEEE Trans. Med. Imag.*, vol. 42, no. 4, pp. 1056–1067, Apr. 2023.

[12] P. Song, J. M. Rubin, and M. R. Lowerison, "Super-resolution ultrasound microvascular imaging: Is it ready for clinical use?" *Zeitschrift für Medizinische Physik*, vol. 33, no. 3, pp. 309–323, Aug. 2023.

[13] S. Dencks and G. Schmitz, "Ultrasound localization microscopy," *Zeitschrift für Medizinische Physik*, vol. 33, no. 3, pp. 292–308, May 2023.

[14] C. Demené et al., "Transcranial ultrafast ultrasound localization microscopy of brain vasculature in patients," *Nature Biomed. Eng.*, vol. 5, no. 3, pp. 219–228, Mar. 2021.

[15] S. Bodard et al., "Ultrasound localization microscopy of the human kidney allograft on a clinical ultrasound scanner," *Kidney Int.*, vol. 103, no. 5, pp. 930–935, May 2023.

[16] L. Denis et al., "Sensing ultrasound localization microscopy for the visualization of glomeruli in living rats and humans," *eBioMedicine*, vol. 91, May 2023, Art. no. 104578.

[17] S. Bodard et al., "Visualization of renal glomeruli in human native kidneys with sensing ultrasound localization microscopy," *Investigative Radiol.*, vol. 59, no. 8, pp. 561–568, Aug. 2024.

[18] C. Huang et al., "Super-resolution ultrasound localization microscopy based on a high frame-rate clinical ultrasound scanner: An in-human feasibility study," *Phys. Med. Biol.*, vol. 66, no. 8, Apr. 2021, Art. no. 08NT01.

[19] F. Knieling, "Ultrasound super-resolution imaging of neonatal cerebral vascular reorganization during neurovascular interventions," *Res. Square*, Nov. 2023, doi: 10.21203/rs.3.rs-3660778/v1.

[20] J. Yan et al., "Transthoracic ultrasound localization microscopy of myocardial vasculature in patients," *Nature Biomed. Eng.*, vol. 8, no. 6, pp. 689–700, May 2024.

[21] J. Zhu et al., "Super-resolution ultrasound localization microscopy of microvascular structure and flow for distinguishing metastatic lymph nodes—An initial human study," *Ultraschall der Medizin-Eur. J. Ultrasound*, vol. 43, no. 6, pp. 592–598, Dec. 2022.

[22] M. Li et al., "Super-resolution ultrasound localization microscopy for the non-invasive imaging of human testicular microcirculation and its differential diagnosis role in male infertility," *View*, vol. 5, no. 2, Apr. 2024, Art. no. 20230093.

[23] T. Opacic et al., "Motion model ultrasound localization microscopy for preclinical and clinical multiparametric tumor characterization," *Nature Commun.*, vol. 9, no. 1, pp. 1–13, Apr. 2018.

[24] A. Chavignon, V. Hingot, C. Orset, D. Vivien, and O. Couture, "3D transcranial ultrasound localization microscopy for discrimination between ischemic and hemorrhagic stroke in early phase," *Sci. Rep.*, vol. 12, no. 1, p. 14607, Aug. 2022.

[25] O. Demeulenaere et al., "Coronary flow assessment using 3-dimensional ultrafast ultrasound localization microscopy," *JACC, Cardiovascular Imag.*, vol. 15, no. 7, pp. 1193–1208, Jul. 2022.

[26] S. B. Andersen et al., "Evaluation of 2D super-resolution ultrasound imaging of the rat renal vasculature using ex vivo micro-computed tomography," *Sci. Rep.*, vol. 11, no. 1, p. 24335, Dec. 2021.

[27] B. Heiles, A. Chavignon, V. Hingot, P. Lopez, E. Teston, and O. Couture, "Performance benchmarking of microbubble-localization algorithms for ultrasound localization microscopy," *Nature Biomed. Eng.*, vol. 6, no. 5, pp. 605–616, Feb. 2022.

[28] M. Lerendegui et al., "ULTRA-SR challenge: Assessment of ultrasound localization and TRacking algorithms for super-resolution imaging," *IEEE Trans. Med. Imag.*, vol. 43, no. 8, pp. 2970–2987, Aug. 2024.

[29] Y. Shin et al., "Context-aware deep learning enables high-efficacy localization of high concentration microbubbles for super-resolution ultrasound localization microscopy," *Nature Commun.*, vol. 15, no. 1, p. 2932, Apr. 2024.

[30] N. Blanken, J. M. Wolterink, H. Delingette, C. Brune, M. Versluis, and G. Lajoinie, "Super-resolved microbubble localization in single-channel ultrasound RF signals using deep learning," *IEEE Trans. Med. Imag.*, vol. 41, no. 9, pp. 2532–2542, Sep. 2022.

[31] H. Belgharbi et al., "An anatomically realistic simulation framework for 3D ultrasound localization microscopy," *IEEE Open J. Ultrason., Ferroelectr., Freq. Control*, vol. 3, pp. 1–13, 2023.

[32] M. A. Averkiou, M. F. Bruce, J. E. Powers, P. S. Sheeran, and P. N. Burns, "Imaging methods for ultrasound contrast agents," *Ultrasound Med. Biol.*, vol. 46, no. 3, pp. 498–517, Mar. 2020.

[33] Y. Desailly, A.-M. Tissier, J.-M. Correas, F. Wintzenrieth, M. Tanter, and O. Couture, "Contrast enhanced ultrasound by real-time spatiotemporal filtering of ultrafast images," *Phys. Med. Biol.*, vol. 62, no. 1, pp. 31–42, Dec. 2016.

[34] V. Hingot, A. Chavignon, B. Heiles, and O. Couture, "Measuring image resolution in ultrasound localization microscopy," *IEEE Trans. Med. Imag.*, vol. 40, no. 12, pp. 3812–3819, Dec. 2021.

[35] V. Hingot, C. Errico, B. Heiles, L. Rahal, M. Tanter, and O. Couture, "Microvascular flow dictates the compromise between spatial resolution and acquisition time in ultrasound localization microscopy," *Sci. Rep.*, vol. 9, no. 1, p. 2456, Feb. 2019.

[36] O. T. von Ramm and S. W. Smith, "Real time volumetric ultrasound imaging system," *J. Digit. Imag.*, vol. 3, no. 4, pp. 261–266, Nov. 1990.

[37] F. Lin, S. E. Shelton, D. Espíndola, J. D. Rojas, G. Pinton, and P. A. Dayton, "3-D ultrasound localization microscopy for identifying microvascular morphology features of tumor angiogenesis at a resolution beyond the diffraction limit of conventional ultrasound," *Theranostics*, vol. 7, no. 1, pp. 196–204, 2017.

[38] J. Zhu et al., "3D super-resolution U.S. imaging of rabbit lymph node vasculature in vivo by using microbubbles," *Radiology*, vol. 291, no. 3, pp. 642–650, Jun. 2019.

[39] M. R. Lowerison et al., "Super-resolution ultrasound reveals cerebrovascular impairment in a mouse model of Alzheimer's disease," *J. Neurosci.*, vol. 44, no. 9, Jan. 2024, Art. no. e1251232024.

[40] İ. Özdemir, K. Johnson, S. Mohr-Allen, K. E. Peak, V. Varner, and K. Hoyt, "Three-dimensional visualization and improved quantification with super-resolution ultrasound imaging—Validation framework for analysis of microvascular morphology using a chicken embryo model," *Phys. Med. Biol.*, vol. 66, no. 8, Apr. 2021, Art. no. 085008.

[41] J. Yin et al., "Pattern recognition of microcirculation with super-resolution ultrasound imaging provides markers for early tumor response to anti-angiogenic therapy," *Theranostics*, vol. 14, no. 3, pp. 1312–1324, 2024.

[42] P. Kruizinga et al., "Compressive 3D ultrasound imaging using a single sensor," *Sci. Adv.*, vol. 3, no. 12, Dec. 2017, Art. no. e1701423.

[43] J. Zhang et al., "Enhancing row-column array (RCA)-based 3D ultrasound vascular imaging with spatial–temporal similarity weighting," *IEEE Trans. Ultrason., Ferroelectr., Freq. control*, Aug. 2024, doi: 10.1109/TMI.2024.3439615.

[44] P. Santos, G. U. Haugen, L. Løvstakken, E. Samset, and J. D'hooge, "Diverging wave volumetric imaging using subaperture beamforming," *IEEE Trans. Ultrason., Ferroelectr., Freq. Control*, vol. 63, no. 12, pp. 2114–2124, Dec. 2016.

[45] P. Guo et al., "A 125 μm-pitch-matched transceiver ASIC with micro-beamforming ADC and multi-level signaling for 3-D transfontanelle ultrasonography," *IEEE J. Solid-State Circuits*, vol. 59, no. 8, pp. 2604–2617, Aug. 2024.

[46] A. Chavignon, B. Heiles, V. Hingot, C. Orset, D. Vivien, and O. Couture, "Deep and complex vascular anatomy in the rat brain described with ultrasound localization microscopy in 3D," *IEEE Open J. Ultrason., Ferroelectr., Freq. Control*, vol. 3, pp. 203–209, 2023.

[47] Y. Desailly, O. Couture, M. Fink, and M. Tanter, "Sono-activated ultrasound localization microscopy," *Appl. Phys. Lett.*, vol. 103, no. 17, Oct. 2013, Art. no. 174107.

[48] M. A. O'Reilly and K. Hynynen, "A super-resolution ultrasound method for brain vascular mapping," *Med. Phys.*, vol. 40, no. 11, Nov. 2013, Art. no. 110707.

[49] Y. Desailly, J. Pierre, O. Couture, and M. Tanter, "Resolution limits of ultrafast ultrasound localization microscopy," *Phys. Med. Biol.*, vol. 60, no. 22, pp. 8723–8740, Nov. 2015.

[50] J. Provost et al., "3D ultrafast ultrasound imaging in vivo," *Phys. Med. Biol.*, vol. 59, no. 19, pp. 1–14, Sep. 2014.

[51] B. Heiles et al., "Ultrafast 3D ultrasound localization microscopy using a 32 × 32 matrix array," *IEEE Trans. Med. Imag.*, vol. 38, no. 9, pp. 2005–2015, Sep. 2019.

[52] B. Heiles et al., "Volumetric ultrasound localization microscopy of the whole rat brain microvasculature," *IEEE Open J. Ultrason., Ferroelectr., Freq. Control*, vol. 2, pp. 261–282, 2022.

[53] D. S. dos Santos et al., "An ultrasound matrix transducer for high-frame-rate 3-D intra-cardiac echocardiography," *Ultrasound Med. Biol.*, vol. 50, no. 2, pp. 285–294, Feb. 2024.

[54] J. A. Jensen et al., "SARUS: A synthetic aperture real-time ultrasound system," *IEEE Trans. Ultrason., Ferroelectr., Freq. Control*, vol. 60, no. 9, pp. 1838–1852, Sep. 2013.

[55] B. Heiles, "3D ultrasound localization microscopy," Ph.D. thesis, Dept. Phys. Med., PSL Res. Univ., Paris, France, Dec. 2019.

[56] O. Demeulenaere et al., "In vivo whole brain microvascular imaging in mice using transcranial 3D ultrasound localization microscopy," *eBioMedicine*, vol. 79, May 2022, Art. no. 103995.

[57] J. R. McCall, F. Santibanez, H. Belgharbi, G. F. Pinton, and P. A. Dayton, "Non-invasive transcranial volumetric ultrasound localization microscopy of the rat brain with continuous, high volume-rate acquisition," *Theranostics*, vol. 13, no. 4, pp. 1235–1246, 2023.

[58] D. H. Turnbull and F. S. Foster, "Beam steering with pulsed two-dimensional transducer arrays," *IEEE Trans. Ultrason., Ferroelectr., Freq. Control*, vol. 38, no. 4, pp. 320–333, Jul. 1991.

[59] F. Foroozan, M. A. O'Reilly, and K. Hynynen, "Microbubble localization for three-dimensional superresolution ultrasound imaging using curve fitting and deconvolution methods," *IEEE Trans. Biomed. Eng.*, vol. 65, no. 12, pp. 2692–2703, Dec. 2018.

[60] L. Deng, H. Lea-Banks, R. M. Jones, M. A. O'Reilly, and K. Hynynen, "Three-dimensional super resolution ultrasound imaging with a multi-frequency hemispherical phased array," *Med. Phys.*, vol. 50, no. 12, pp. 7478–7497, Dec. 2023.

[61] E. Boni et al., "ULA-OP 256: A 256-channel open scanner for development and real-time implementation of new ultrasound methods," *IEEE Trans. Ultrason., Ferroelectr., Freq. Control*, vol. 63, no. 10, pp. 1488–1495, Oct. 2016.

[62] S. Harput et al., "3-D super-resolution ultrasound imaging with a 2-D sparse array," *IEEE Trans. Ultrason., Ferroelectr., Freq. Control*, vol. 67, no. 2, pp. 269–277, Feb. 2020.

[63] A. Ramalli, E. Boni, A. S. Savoia, and P. Tortoli, "Density-tapered spiral arrays for ultrasound 3-D imaging," *IEEE Trans. Ultrason., Ferroelectr., Freq. Control*, vol. 62, no. 8, pp. 1580–1588, Aug. 2015.

[64] J. Robin, A. Özbek, M. Reiss, X. L. Dean-Ben, and D. Razansky, "Dual-mode volumetric optoacoustic and contrast enhanced ultrasound imaging with spherical matrix arrays," *IEEE Trans. Med. Imag.*, vol. 41, no. 4, pp. 846–856, Apr. 2022.

[65] M. Bernal, B. Cunitz, D. Rohrbach, and R. Daigle, "High-frame-rate volume imaging using sparse-random-aperture compounding," *Phys. Med. Biol.*, vol. 65, no. 17, Sep. 2020, Art. no. 175002.

[66] L. Peralta, D. Mazierli, A. Gomez, J. V. Hajnal, P. Tortoli, and A. Ramalli, "3-D coherent multitransducer ultrasound imaging with sparse spiral arrays," *IEEE Trans. Ultrason., Ferroelectr., Freq. Control*, vol. 70, no. 3, pp. 197–206, Mar. 2023.

[67] A. Chavignon, B. Heiles, V. Hingot, C. Orset, D. Vivien, and O. Couture, "3D transcranial ultrasound localization microscopy in the rat brain with a multiplexed matrix probe," *IEEE Trans. Biomed. Eng.*, vol. 69, no. 7, pp. 2132–2142, Jul. 2022.

[68] U.-W. Lok et al., "Three-dimensional ultrasound localization microscopy with bipartite graph-based microbubble pairing and Kalman-filtering-based tracking on a 256-channel Verasonics ultrasound system with a 32 × 32 matrix array," *J. Med. Biol. Eng.*, vol. 42, no. 6, pp. 767–779, Oct. 2022.

[69] J. Yan et al., "Fast 3D super-resolution ultrasound with adaptive weight-based beamforming," *IEEE Trans. Biomed. Eng.*, vol. 70, no. 9, pp. 2752–2761, Mar. 2023.

[70] K. Riemer et al., "3D acoustic wave sparsely activated localization microscopy with phase change contrast agents," *Investigative Radiol.*, vol. 59, no. 5, pp. 379–390, May 2024.

[71] C. Bourquin et al., "Quantitative pulsatility measurements using 3D dynamic ultrasound localization microscopy," *Phys. Med. Biol.*, vol. 69, no. 4, Feb. 2024, Art. no. 045017.

[72] N. Ghigo et al., "Dynamic ultrasound localization microscopy without ECG-gating," *Ultrasound Med. Biol.*, vol. 50, no. 9, pp. 1436–1448, Sep. 2024.

[73] P. Xing, V. Perrot, A. U. Dominguez-Vargas, S. Quessy, N. Dancause, and J. Provost, "Towards transcranial 3D ultrasound localization microscopy of the nonhuman primate brain," 2024, *arXiv:2404.03547*.

[74] A. Coudert, A. Chavignon, L. Denis, and O. Couture, "Volumetric ultrasound localization microscopy with diverging cylindrical waves," *IEEE Trans. Ultrason., Ferroelectr., Freq. Control*, early access, Mar. 11, 2024, doi: 10.1109/TUFFC.2024.3375896.

[75] A. Coudert et al., "3D transcranial ultrasound localization microscopy reveals major arteries in the sheep brain," *IEEE Trans. Ultrason., Ferroelectr., Freq. Control*, early access, Jul. 25, 2024, doi: 10.1109/TUFFC.2024.3432998.

[76] J. R. McCall et al., "Longitudinal 3-D visualization of microvascular disruption and perfusion changes in mice during the evolution of glioblastoma using super-resolution ultrasound," *IEEE Trans. Ultrason., Ferroelectr., Freq. Control*, vol. 70, no. 11, pp. 1401–1416, Nov. 2023.

[77] J. R. McCall, A. Chavignon, O. Couture, P. A. Dayton, and G. F. Pinton, "Element position calibration for matrix array transducers with multiple disjoint piezoelectric panels," *Ultrason. Imag.*, vol. 46, no. 3, pp. 139–150, Feb. 2024.

[78] J. Jensen et al., "Three-dimensional super-resolution imaging using a row–column array," *IEEE Trans. Ultrason., Ferroelectr., Freq. control*, vol. 67, no. 3, pp. 538–546, Oct. 2019.

[79] C. Hyung Seo and J. T. Yen, "A 256 × 256 2-D array transducer with row-column addressing for 3-D rectilinear imaging," *IEEE Trans. Ultrason., Ferroelectr., Freq. Control*, vol. 56, no. 4, pp. 837–847, Apr. 2009.

[80] M. Flesch et al., "4D in vivo ultrafast ultrasound imaging using a row-column addressed matrix and coherently-compounded orthogonal plane waves," *Phys. Med. Biol.*, vol. 62, no. 11, pp. 4571–4588, Jun. 2017.

[81] M. F. Rasmussen, T. L. Christiansen, E. V. Thomsen, and J. A. Jensen, "3-D imaging using row-column-addressed arrays with integrated apodization—Part I: Apodization design and line element beamforming," *IEEE Trans. Ultrason., Ferroelectr., Freq. Control*, vol. 62, no. 5, pp. 947–958, May 2015.

[82] M. L. Ommen, M. Schou, C. Beers, J. A. Jensen, N. B. Larsen, and E. V. Thomsen, "3D printed calibration micro-phantoms for super-resolution ultrasound imaging validation," *Ultrasonics*, vol. 114, Jul. 2021, Art. no. 106353.

[83] J. Jensen et al., "Anatomic and functional imaging using row-column arrays," *IEEE Trans. Ultrason., Ferroelectr., Freq. control*, vol. 69, no. 10, pp. 2722–2738, Jul. 2022.

[84] J. Hansen-Shearer et al., "Ultrafast 3-D transcutaneous super resolution ultrasound using row-column array specific coherence-based beamforming and rolling acoustic sub-aperture processing: In vitro, in rabbit and in human study," *Ultrasound Med. Biol.*, vol. 50, no. 7, pp. 1045–1057, Jul. 2024.

[85] M. Caudoux et al., "Curved toroidal row column addressed transducer for 3D ultrafast ultrasound imaging," *IEEE Trans. Med. Imag.*, vol. 43, no. 9, pp. 3279–3291, Sep. 2024.
[86] A. Bertolo, J. Sauvage, M. Tanter, M. Pernot, and T. Deffieux, "XDoppler: Cross-correlation of orthogonal apertures for 3D blood flow imaging," *IEEE Trans. Med. Imag.*, vol. 40, no. 12, pp. 3358–3368, Dec. 2021.
[87] M. Audoin, A. Salari, B. G. Tomov, K. F. Pedersen, J. A. Jensen, and E. V. Thomsen, "Diverging polymer acoustic lens design for high-resolution row–column array ultrasound transducers," *IEEE Trans. Ultrason., Ferroelectr., Freq. Control*, vol. 71, no. 1, pp. 202–213, Jan. 2024.
[88] H. Favre, M. Pernot, M. Tanter, and C. Papadacci, "Boosting transducer matrix sensitivity for 3D large field ultrasound localization microscopy using a multi-lens diffracting layer: A simulation study," *Phys. Med. Biol.*, vol. 67, no. 8, Apr. 2022, Art. no. 085009.
[89] H. Favre, M. Pernot, M. Tanter, and C. Papadacci, "Transcranial 3D ultrasound localization microscopy using a large element matrix array with a multi-lens diffracting layer: An *invitro* study," *Phys. Med. Biol.*, vol. 68, no. 7, Apr. 2023, Art. no. 075003.
[90] J. R. McCall, P. A. Dayton, and G. F. Pinton, "Characterization of the ultrasound localization microscopy resolution limit in the presence of image degradation," *IEEE Trans. Ultrason., Ferroelectr., Freq. Control*, vol. 69, no. 1, pp. 124–134, Jan. 2022.
[91] B. Rauby, P. Xing, J. Porée, M. Gasse, and J. Provost, "Pruning sparse tensor neural networks enables deep learning for 3D ultrasound localization microscopy," 2024, *arXiv:2402.09359*.
[92] C. Orset et al., "Mouse model of in situ thromboembolic stroke and reperfusion," *Stroke*, vol. 38, no. 10, pp. 2771–2778, Oct. 2007.
[93] Y. Tang et al., "Non-invasive deep-brain imaging with 3D integrated photoacoustic tomography and ultrasound localization microscopy (3D-PAULM)," *IEEE Trans. Med. Imag.*, early access, Oct. 9, 2024, doi: 10.1109/TMI.2024.3477317.
[94] L. Wei et al., "High-frame-rate volumetric porcine renal vasculature imaging," *Ultrasound Med. Biol.*, vol. 49, no. 12, pp. 2476–2482, Dec. 2023.
[95] G. Chabouh et al., "Whole organ volumetric sensing ultrasound localization microscopy for characterization of kidney structure," *IEEE Trans. Med. Imag.*, early access, Jun. 10, 2024, doi: 10.1109/TMI.2024.3411669.
[96] C. Papadacci et al., "4D simultaneous tissue and blood flow Doppler imaging: Revisiting cardiac Doppler index with single heart beat 4D ultrafast echocardiography," *Phys. Med. Biol.*, vol. 64, no. 8, Apr. 2019, Art. no. 085013.
[97] C. Zhang et al., "Evaluation of tumor microvasculature with 3D ultrasound localization microscopy based on 2D matrix array," *Eur. Radiol.*, vol. 34, no. 8, pp. 5250–5259, Jan. 2024.
[98] S. Lei et al., "In vivo ocular microvasculature imaging in rabbits with 3D ultrasound localization microscopy," *Ultrasonics*, vol. 133, Aug. 2023, Art. no. 107022.
[99] S. Bae, S. Lee, and E. Konofagou, "Detection of blood volume reduction and vasoconstriction following focused ultrasound blood-brain barrier opening using ultrasound flow imaging," *BioRxiv*, Oct. 2023, doi: 10.1101/2023.10.19.563176.
[100] N. Renaudin, C. Demené, A. Dizeux, N. Ialy-Radio, S. Pezet, and M. Tanter, "Functional ultrasound localization microscopy reveals brain-wide neurovascular activity on a microscopic scale," *Nature Methods*, vol. 19, no. 8, pp. 1004–1012, Aug. 2022.
[101] E. Roux, F. Varray, L. Petrusca, C. Cachard, P. Tortoli, and H. Liebgott, "Experimental 3-D ultrasound imaging with 2-D sparse arrays using focused and diverging waves," *Sci. Rep.*, vol. 8, no. 1, p. 9108, Jun. 2018.
[102] G. Li et al., "A single crystal row–column-array for 3D ultrasound imaging," *Ultrasonics*, vol. 139, Apr. 2024, Art. no. 107289.
[103] Y. Qiu et al., "Piezoelectric micromachined ultrasound transducer (PMUT) arrays for integrated sensing, actuation and imaging," *Sensors*, vol. 15, no. 4, pp. 8020–8041, Apr. 2015.
[104] O. Oralkan et al., "Volumetric ultrasound imaging using 2-D CMUT arrays," *IEEE Trans. Ultrason., Ferroelectr., Freq. Control*, vol. 50, no. 11, pp. 1581–1594, Nov. 2003.
[105] C. Huang et al., "Short acquisition time super-resolution ultrasound microvessel imaging via microbubble separation," *Sci. Rep.*, vol. 10, no. 1, p. 6007, Apr. 2020.
[106] R. Tenajas, D. Miraut, C. I. Illana, R. Alonso-Gonzalez, F. Arias-Valcayo, and J. L. Herraiz, "Recent advances in artificial intelligence-assisted ultrasound scanning," *Appl. Sci.*, vol. 13, no. 6, p. 3693, Mar. 2023.
[107] M. Moeini et al., "Compromised microvascular oxygen delivery increases brain tissue vulnerability with age," *Sci. Rep.*, vol. 8, no. 1, p. 8219, May 2018.
[108] L. Østergaard, "Blood flow, capillary transit times, and tissue oxygenation: The centennial of capillary recruitment," *J. Appl. Physiol.*, vol. 129, no. 6, pp. 1413–1421, Dec. 2020.
[109] F. N. Soria, C. Miguelez, O. Peñagarikano, and J. Tønnesen, "Current techniques for investigating the brain extracellular space," *Frontiers Neurosci.*, vol. 14, Oct. 2020, Art. no. 570750.
[110] P. Ehrenfest, "In what way does it become manifest in the fundamental laws of physics that space has three dimensions," *Proc. Amsterdam Acad.*, vol. 20, no. 1, p. 200, Dec. 1917.
[111] Q. Zhou, K. H. Lam, H. Zheng, W. Qiu, and K. K. Shung, "Piezoelectric single crystal ultrasonic transducers for biomedical applications," *Prog. Mater. Sci.*, vol. 66, pp. 87–111, Oct. 2014.
[112] J. D. Larson, "2-D phased array ultrasound imaging system with distributed phasing," U.S. Patent 5 229 933, Jul. 20, 1993.
[113] G. Chabouh et al., "RF channel-based adaptive beamforming for 3D ultrasound localization microscopy," *BioRxiv*, Aug. 2024, doi: 10.1101/2024.08.02.606290.
[114] G. Chabouh, "An open-source platform for 3D transcranial ultrasound localization microscopy in awake mice," *Res. Square*, Sep. 2024, doi: 10.21203/rs.3.rs-4925712/v1.
[115] G. Montaldo, D. Palacio, M. Tanter, and M. Fink, "Time reversal kaleidoscope: A smart transducer for three-dimensional ultrasonic imaging," *Appl. Phys. Lett.*, vol. 84, no. 19, pp. 3879–3881, May 2004.
[116] O. Caron-Grenier, J. Poree, V. Perrot, G. Ramos-Palacio, A. F. Sadikot, and J. Provost, "Ergodic encoding for single-element ultrasound imaging in vivo," 2023, *arXiv:2308.09196*.

Louise Denis (Member, IEEE) was born in Paris, France, in 1997. She received the M.Sc. degree in biomedical engineering from the Engineering School, ECE Paris, in 2020, and the Ph.D. degree from the Laboratoire d'Imagerie Biomédicale, Sorbonne Université, Paris, in 2023, under the supervision of Dr. Olivier Couture, on the transfer of 2-D ultrasound localization microscopy (ULM) to several clinical applications (brain and kidney).

She did several internships in the fields of quantitative ultrasound (Physics for Medicine, Paris) and therapeutic ultrasound (LabTau, Lyon, France). She is currently a Postdoctoral Researcher with the Laboratoire d'Imagerie Biomédicale, Sorbonne Université, working on several applications of 3-D ultrasound localization microscopy, including a clinical study on the human brain.

Dr. Denis received the French Young Talent Award from the Fondation l'Oreal—UNESCO (for Women in Science) in 2023.

Georges Chabouh (Member, IEEE) received an M.Sc. in mechanical engineering, with a double Diploma from both the Lebanese University Faculty of Engineering (ULFG-II), Beirut, Lebanon, and Institut National des Sciences Appliquees (INSA), Toulouse, France, in 2018. He then obtained a Master of Research in fluid dynamics, energetics, and heat transfer. He received the Ph.D. degree from the Université Grenoble Alpes, Grenoble, France, in 2022, focusing on novel targeted drug delivery using microbubble shell buckling technology.

Subsequently, he joined Olivier Couture's Laboratory at Sorbonne University, Paris, France, to develop 3-D ultrasound localization microscopy (ULM) for stroke treatment and volumetric segmentation of kidney glomeruli. He is currently an Associate Research Scientist at Columbia University, New York, NY, USA, working with Prof. Elisa Konofagou, on blood–brain barrier opening techniques for treating neurodegenerative diseases.

Dr. Chabouh received the PEPS CNRS Award "La Mécanique du Futur" in 2022 and chaired the Gordon Research Seminar on Tissue Microstructure Imaging in 2023.

Baptiste Heiles (Member, IEEE) received the M.Sc. degree in general and civil engineering from Ecole Normale Superieure Paris Saclay, Cachan, France, in 2013, the agrégation de Sciences Industrielles degree from École Normale Supérieure de Cachan, Cachan, in 2014, the Master of Research degree in fluid mechanics and heat transfers from Ecole Centrale de Paris, Châtenay-Malabry, France, in 2015, and the Ph.D. degree from the Physics for Medicine, Paris, France, in 2019, supervised by Dr. Olivier Couture.

His Ph.D. research centered on enhancing ULM in traditional 2-D imaging for preclinical and clinical work, as well as introducing 3-D ULM. This enabled the first demonstration of detailed images of the rat brain microvasculature in vivo with a resolution of a dozen microns. In 2020, he joined David Maresca at the Department of Imaging Physics, Technische Universiteit Delft, Delft, The Netherlands. He has worked on enhancing nonlinear imaging for synthetic and genetically encoded contrast agents and developing novel approaches for contrast-enhanced ultrasound data simulation with a strong focus on ultrasound super-resolution. He has engineered sound-sheet imaging, a fast volumetric method to image endogenous and genetically encoded and synthetic contrast agents. He is currently with Prof. Mikhail Shapiro at Caltech, Pasadena, CA, USA.

Dr. Heiles was awarded a Marie-Sklodowska Curie Actions Fellowship for his project entitled Multi-messenger Imaging of Cancer in 2022.

Olivier Couture (Member, IEEE) was born in Quebec City, Canada, in 1978. He received the B.Sc. degree in physics from McGill University, Montreal, QC, Canada, in 2001, the Ph.D. degree from the Department of Medical Biophysics, University of Toronto, Toronto, ON, Canada, in 2007, and the Habilitation (HDR) degree from Universite Paris Diderot, Paris, France, in 2017.

After a postdoctoral fellowship at ESPCI, Paris, he was hired as a Tenured Research Associate at CNRS, based within the Langevin Institute, Paris. Following a promotion to CNRS Research Director in 2019, he moved to the Laboratoire d'Imagerie Biomedicale, Sorbonne Universite, Paris, to head the team Physiology and Pathology of the Microcirculation.

Dr. Couture was awarded the "2017 IEEE Ultrasonics Early Career Investigation Award" for the development of ultrasound super-resolution and plane-wave contrast imaging. He received the ERC Consolidator Grant for the application of ultrasound localization microscopy to stroke diagnosis. He initiated the short course on super-resolution ultrasound at IEEE IUS in 2020 and helped launch the corresponding track. He will be the Chair of the Gordon Research Conference on Tissue Microstructure Imaging in 2025.